The structure of a working catalyst ; from flat surfaces to nanoparticles

Roobol, S.B.

Chapter 7

Oxide shell formation during spontaneous oscillations in the catalytic oxidation of CO on palladium nanoparticles

Spontaneous reaction oscillations on palladium nanoparticles during the catalytic oxidation of CO have been investigated by a combination of in-situ microscopy techniques and X-ray scattering. The oscillations are identified as sequences of switches between a high- and a low-reactivity phase and vice versa. The high-reactivity phase is accompanied by the presence of a 1 nm thick palladium oxide shell that encapsulates the metallic core of each particle. Based on this observation, a mechanism is proposed for the oscillations that involves the catalytic activity and the stability of the palladium oxide.

The work presented in this chapter has been performed together with Willem Onderwaater.

7.1 Introduction

Spontaneous reaction oscillations have been observed for many heterogeneous catalytic systems, ranging from single-crystal model systems in ultrahigh vacuum [124], to thin films[125], supported nanoparticle systems[126], and even up to commercial reactors such as automotive catalytic converters[127]. Only for a few single-crystal model systems, atomic-scale mechanisms for reaction oscillations have been studied in detail[94, 128–131]. In this chapter, spontaneous oscillations during CO oxidation on Pd nanoparticles, supported on flat substrates, are investigated with a variety of techniques. The measurements suggest that the oscillation mechanism on the particles could be similar to that on Pd single-crystal surfaces.

In previous work on the Pd(100) surface[131], a high-pressure mechanism has been identified that features a refined interplay between variations in the step density or surface roughness, the stability of the PdO surface oxide (which depends on the surface roughness and the local gas composition), and the catalyst activity (which in turn depends on the state of the surface). A full cycle of the oscillation on Pd(100) proceeds as follows. The reaction takes place under conditions that are so oxygen-rich that the smooth metal surface is unstable with respect to oxidation. As a consequence, a thin surface oxide is formed. The oxidised surface is more reactive than the metal, causing a higher consumption of CO and thus a drop in CO partial pressure as soon as the formation of the surface oxide starts. This locally accelerates the oxidation and makes it synchronise across the whole surface. In the oxide phase, the reaction follows the Mars-Van Krevelen mechanism[132]: CO adsorbs on the surface oxide, and reacts with this oxide to form CO_2. In this process, some of the Pd atoms get reduced and become mobile, diffusing out on top of the oxide until they get re-oxidised, thereby increasing the surface roughness. Eventually, this roughness destabilises the surface oxide and the systems switches back to a rough metallic surface. The reason for this is thought to be that the CO binds even more strongly to the step sites on the metal surface than to terrace sites. This increasingly favours the metal surface as roughening on the oxide progresses. The lower activity of the metal surface makes the CO partial pressure increase again, now further stabilizing the metal surface. The high surface mobility of the metal surface leads to a swift smoothening. This removes the binding advantage of CO to the step sites and makes the metal surface instable again, causing the whole process to start over again.

Oscillating nanoparticle catalyst systems have been reported, but there have been few attempts to systematically investigate the precise oscillation mechanisms. Detailed mass spectrometry analysis of oscillations during CO oxidation on platinum particles by Jensen and co-workers[133] suggested that the surface-transition mechanism described above for Pd(100) could also apply to these nanoparticles. However, the roughness of an extended surface is a property that is difficult to

translate to a nanoparticle, and such a "translation" has not been performed in ref. [133]. Also on Pt particles, in an in-situ Transmission Electron Microscopy (TEM) study[118], particle morphology variations have been observed that correlate with the oscillations. By employing mass transport simulations and DFT, the conclusion was drawn that the oscillations are the result of a bistability in the Langmuir-Hinselwood kinetics.

The interaction of oxygen with palladium nanoparticles has been studied on Fe_3O_4 substrates[134–136], on Al_2O_3[137, 138], and for epitaxially aligned particles on MgO[139], both at low and high O_2 pressures, and also in the context of CO oxidation. Nevertheless, oscillations in the CO oxidation rate on Pd nanoparticles have not been reported before.

7.2 Methods

In order to acquire as much structural information as possible, under actual, high-pressure, high-temperature conditions, we have employed a combination of four complementary structurally sensitive techniques, each under operando conditions.

High-pressure X-ray Diffraction (XRD) experiments have been conducted in the special, 17 ml flow-reactor setup that has been installed at the ID03 beamline of the European Synchrotron Radiation Facility (ESRF), especially for surface X-ray diffraction under catalytic conditions[22]. These experiments reveal which structural components, e.g. metal or oxide, are present. The same setup has been used to perform Grazing-Incidence Small-Angle X-ray Scattering (GISAXS) measurements on the Pd particles, which provides information on the average spatial arrangement of individual particles and is sensitive to the presence of e.g. core-shell structures[140].

A direct, real-space view of Pd nanoparticles under reaction conditions has been obtained with two in-situ microscopy techniques. We have conducted in-situ, non-contact Atomic Force Microscopy (AFM) experiments, using the new *ReactorAFM* setup with its 0.5 ml reactor volume, described in detail in chapter 2 and ref. [46]. These observations give information on the irreversible changes, such as ripening or sintering, and on reversible changes in the shapes and heights of the nanoparticles during reaction oscillations. The AFM observations have been complemented by extensive high-pressure TEM observations, where we have made use of the especially developed nanoreactors, which we also used in chapter 6 and which are described in refs. [13, 23]. The experiments were performed at 300 keV using an FEI Titan microscope at Delft University of Technology.

For the X-ray and AFM experiments, the nanoparticles had to be supported on a flat substrate. Samples with well-defined densities, (100/ μm^2 for the AFM, 700/ μm^2 for the X-ray experiments), of size-selected Pd particles generated using

a spark discharge method (average diameter of 6 nm for AFM and 15 nm for the X-rays) supported on a flat $\alpha-Al_2O_3$ substrate, were kindly provided by Dr. M.E. Messing and Prof. K. Deppert and co-workers from Lund University in Sweden[40]. For the TEM experiments the nanoreactor was loaded with palladium nitrate salt. After oxidation with O_2 at 300°C and reduction by H_2 at 500°C, Pd nanoparticles had formed with sizes ranging from 5 to 50 nm.

Like the X-ray flow-reactor setup, the *ReactorAFM* operates in flow mode using a combination of mass flow controllers and back pressure controllers, typically operating with residence times of 5 to 20 seconds. The X-ray flow reactor has an adjustable leak to the UHV system which also contains the quadrupole mass spectrometer (QMS), resulting in gas composition measurement without any delay. For the *ReactorAFM*, the gas analysis is performed downstream by a (QMS-based) T100 analyser from LPM[120]. This configuration introduces a delay of a few seconds, but does not suffer from a loss in time resolution, thanks to the small volume of the input stage of the T100 analyser. However, the flow through a TEM nanoreactor is too small to be controlled with a commercial flow regulator, and the nanoreactors have been operated by defining a certain pressure of a gas mixture at the inlet and feeding the outlet directly into the differentially pumped ultra-high vacuum system (UHV) of a T100 analyser. Because of the micrometre-scaled dimensions of the nanoreactor, the pressure drops completely to zero over the length of the reactor, and the flow through the reactor can be handled directly by a turbomolecular pump. The second turbomolecular pump on the UHV system maintains the optimal working pressure for the QMS. The large volume of the capillary from the nanoreactor to the gas analyzer compared to the flow results in a time resolution for gas detection of approximately 30 s.

7.3 Results and discussion

In this section the experimental results are presented. We start with the crystallographic information derived from the XRD experiments. After addressing the particle shapes with TEM and AFM, we analyse the GISAXS patterns to obtain a detailed view of the rearrangement of the Pd nanoparticles during the catalytic reaction oscillations.

Although the different experimental techniques have been applied under different conditions, all data have been obtained close to the metal/surface oxide boundary, as indicated in figure 7.1.

7.3.1 X-ray diffraction

The upper panel of figure 7.2 shows the periodic variations in the CO_2 and CO partial pressures during spontaneous reaction oscillations on size-selected 15 nm Pd

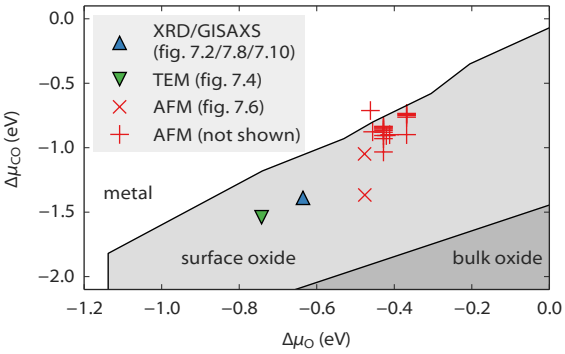

Figure 7.1. Experimental conditions of all experiments reported in this chapter, expressed in terms of the chemical potentials of carbon monoxide and oxygen. The three greylevels indicate three of the phases of a Pd(100) surface in contact with CO and O_2, as calculated using DFT by Rogal et al[141]. Since a nanoparticle exposes multiple different facets, it is to be expected that the phase boundaries for a nanoparticle system will be in slightly different positions. The phase boundaries will also shift and blur because of the CO oxidation reaction itself[142]. The two triangles correspond to observed reaction oscillations, indicating that these points are near a phase boundary, whereas only microscopy images but no reactivity data could be obtained for the cross markers.

particles on $\alpha-Al_2O_3$ in the 17 ml XRD flow cell. The nanoparticles were exposed to a constant gas flow of 60 ml_n/min consisting of CO, O_2 and Ar, at partial pressures of 9, 210, and 281 mbar respectively. The sample was heated at constant power to a temperature of about 588 K. The XRD measurements that were taken simultaneously with the mass spectrometry data exhibited periodic variations in the diffraction intensities at angles corresponding to either the crystal structure of metallic Pd or that of PdO. These variations were out of phase with each other; when the Pd signal was high, the PdO signal was low and vice versa. These oscillations were fully synchronised with those in the CO and CO_2 partial pressures. Figure 7.2 shows that the high-reactivity phase coincided with the presence of the oxide. The sample temperature varied in response to the changes in the turnover rate, since CO oxidation is an exothermic reaction. The oscillations had a period of a few minutes, depending on the temperature, and could be sustained indefinitely within the time scale accessible in our synchrotron experiments. The presence of the X-ray beam only quantitatively affects the oscillations: without the beam the oscillation period is a factor 2 longer and the amplitude of the temperature variations increases by 50%.

In addition to XRD, GISAXS experiments have been performed. Figure 7.2 shows that also the GISAXS signal varied synchronously with the reaction oscillation. These variations will be addressed in more detail in section 7.3.4.

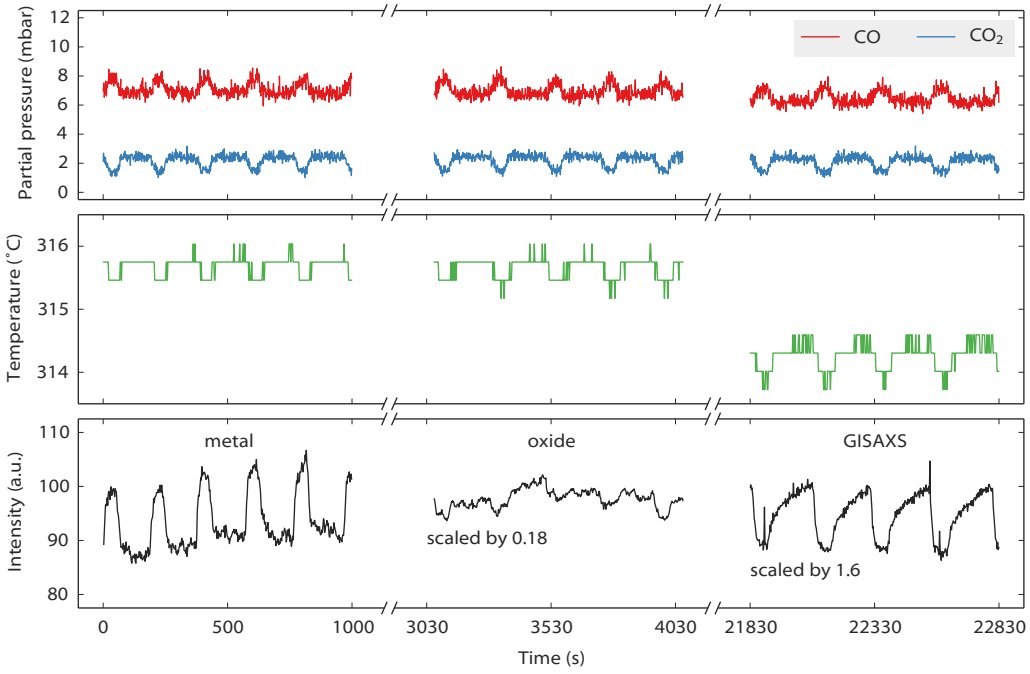

Figure 7.2. Spontaneous reaction oscillations observed using X-ray scattering. The upper panel shows the CO and CO_2 partial pressures as a function of time. The middle panel shows (a low resolution measurement of) the sample temperature. The gas feed was kept constant at 9 mbar CO, 210 mbar O_2, and 281 mbar Ar at a total flow of 60 ml_n/min, and the sample heater was operated at a constant power (its value was adjusted slightly around t = 20 000 s). Note that the absolute value of the partial pressures of CO and CO_2 contains an error due to varying background level for these gases in the mass spectrometer. The amplitude of the oscillations in these signals is not affected by this. The lower panel shows the periodic intensity variations in three different X-ray signals: the metal Pd peak at the 2θ = 17.6° diffraction angle, the oxide PdO peak at 2θ = 15° (see also figure 7.3), and the integrated intensity from a region in a series of GISAXS patterns (see figure 7.8). A high metal intensity is correlated with a low turnover rate, whereas a high oxide intensity correlates with a high turnover rate. Also the changes in the GISAXS signal are synchronised with the reaction oscillations.

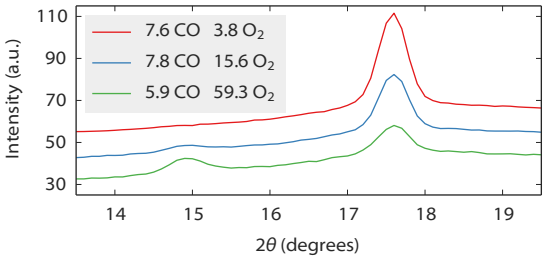

Figure 7.3. X-ray diffraction patterns of the Pd nanoparticles in three different mixtures of O_2 and CO at a total pressure of 200 mbar and a temperature of 375°C. The CO and O_2 partial pressures in mbar are indicated in the legend, the rest of the atmosphere consisted of argon. The patterns are offset by 10 a.u. for clarity. The peak at $2\theta = 17.6°$ corresponds to the (111) reflection of metallic Pd, $2\theta = 15°$ corresponds to the (101) reflection of the oxide PdO.

7.3.2 Transmission electron microscopy

In-situ TEM has been used to obtain a direct view in real space of Pd nanoparticles during oscillations in CO oxidation at atmospheric pressures and elevated temperatures.

In the employed configuration of nanoreactor gas lines, QMS system and vacuum pumping, the residence time of gas in the 0.4 nl reactor was less than 1 ms, and the sensitivity of the reaction product detection was sufficient to measure CO conversion, although the time resolution was only about 30 s, due to diffusive mixing of the gases between reactor and mass spectrometer. In addition to reactivity measurements, the TEM nanoreactor allows sensitive calorimetric measurements with a time resolution of 0.5 s, and this was our primary detection method for the oscillations. The reactor was operated at constant temperature using an electronic feedback circuit, and since the CO oxidation reaction is exothermic, the high-reactivity regime corresponded to lower power input from the sample heater, while the low-activity regime corresponded to higher heating power.

When operating at elevated temperature, there were large temperature gradients in the region around the electron-transparent windows that need to be taken in consideration. Measurements on an earlier version of the nanoreactor[143] and simulations on the current version[118] showed that when operating the heater at a setpoint of 723 K, the center of the heated region was typically 50 K hotter, while the electron-transparent windows, which are situated near the edge of the heated zone, were typically 100 K colder than the value measured from the resistance of the heater.

The nanoreactor was loaded with 5 to 50 nm nanoparticles, as described in section 7.2. When exposing these particles to a mixture of 33 mbar CO and 217 mbar O_2 at temperatures near 400°C, spontaneous reaction oscillations occured as can

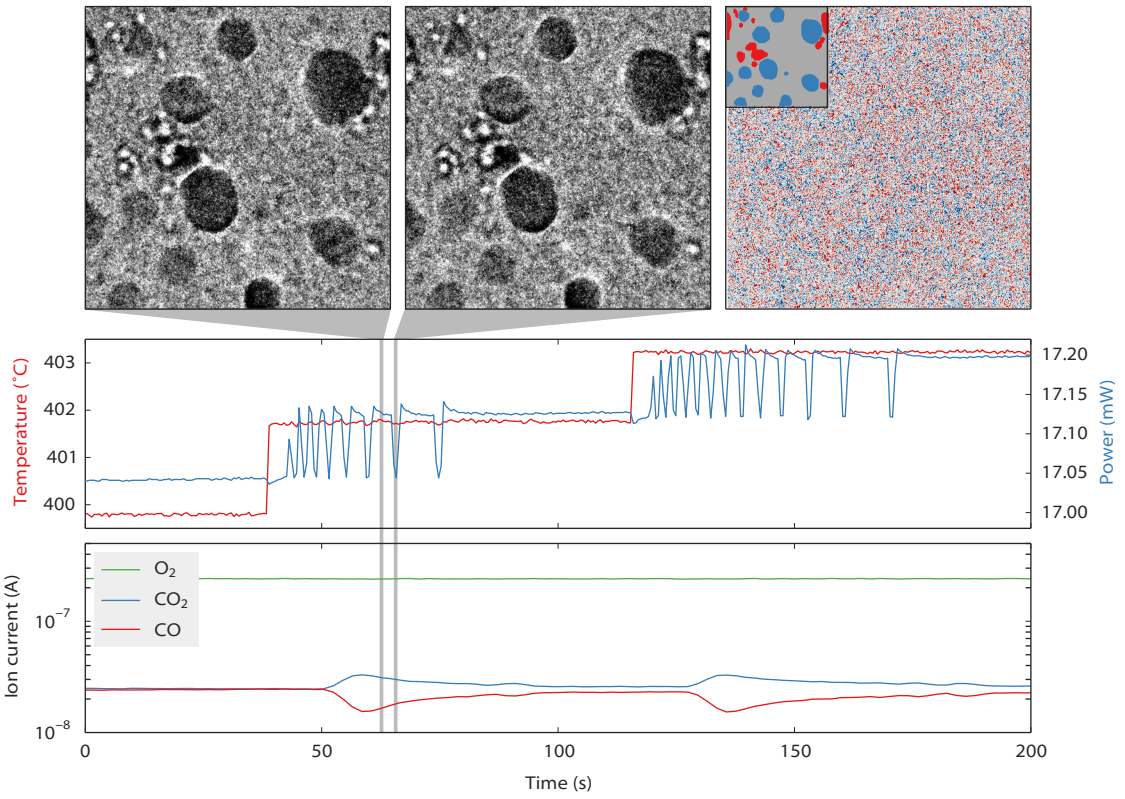

Figure 7.4. (Upper panels) TEM observations during reaction oscillations, $98 \times 98\ \mathrm{nm}^2$ field of view. The first image was taken in the low-reactivity regime, and the second image, which was taken 3 s later than the first, was taken in the high-reactivity regime. The third image shows the difference image (after drift correction) between the first and second image, with the inset indicating in blue the particles that were in focus, and in red the particles on the other window of the nanoreactor that were out of focus. (Middle panel) Sample temperature and required heating power. After both temperature steps, the system exhibited a finite number of reaction oscillations, as can be read off from the heating power variations. (Lower panel) Mass spectrometry signals. The time resolution of the gas detection system was not good enough to resolve the oscillations, even though the partial pressures of CO and CO_2 do reflect the average effect of a burst of oscillations, at t = 40 and t = 120 s.

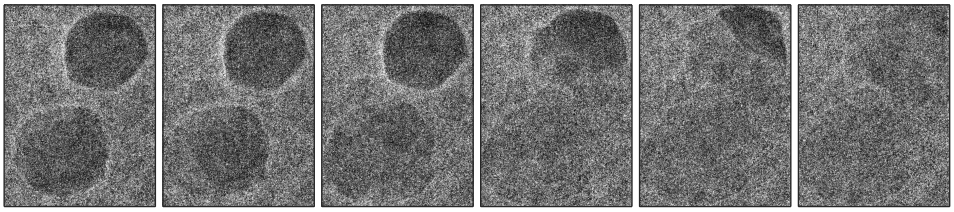

Figure 7.5. Bulk oxidation of Pd particles in 250 mbar O_2 at 400°C, imaged with 30 e/Å^{2}s. A single oxidation front passed through both particles. Note the reduced contrast after oxidation due to the lower density of PdO with respect to that of pure Pd. Each image measures 33×44 nm^2.

be seen in the time dependence of the heater power shown in figure 7.4.

In contrast to the X-ray experiments, the oscillations could not be sustained for prolonged times. After the oscillations started, either spontaneously or triggered by a small temperature increase in the order of 1 K, the system continued oscillating for at most several minutes. Typically, the period of the oscillations continuously increased from 2 to 15 seconds over the course of 10 to 100 periods, before coming to a halt in the low-reactivity regime. We attribute the shorter period and the reduced lifetime of the oscillations compared to those in the SXRD reactor to the higher temperature in the TEM experiments, as the processes that determine the time scale of the oscillations (for the Pd(100) surface these were the roughening and annealing), are likely to take place at a faster rate at the higher temperature. Also the wider particle size distribution could play a role, as these processes might come to a halt earlier on small particles causing the system to switch to the other regime.

Figure 7.4 shows two TEM images of Pd particles in a downstream window, taken in consecutive low- and high-reactivity phases. The difference image shows absolutely no features above the noise. This shows that the TEM images cannot resolve any changes in the particle morphology. Due to the low signal-to-noise ratio of the particles on the speckled background (from the amorphous SiN nanoreactor windows), and due to the Fresnel scattering halo around each particle perimeter, the effective resolution in our images was limited to values not better than 0.5 nm for metallic Pd, and 1 nm for PdO, due to its lower density.

The images in figure 7.4 have been taken with an electron flux of 30 e/Å^{2}s. Higher current densities have been observed to inhibit bulk oxidation of Pd, but we have verified that at the current density of our experiment the Pd particles could oxidise completely in pure oxygen (figure 7.5).

Due to the existence of large temperature gradients in the reactor, it is possible that the region imaged in these experiments was actually not participating in the reaction oscillations. The central hot region might have been oscillating, while the particles downstream of the hot zone and (which experience nearly the same

gas conditions but are at 100-150°C lower temperature), might have behaved differently. Unfortunately, there were no electron-transparent windows in the hot zone. Also, no difference has been observed between particles in windows upstream and downstream of the hot zone.

7.3.3 Atomic force microscopy

Whereas TEM gives high-resolution cross-sectional information on the nanoparticles, height information is mostly inaccessible. In addition, the Pd particles in the nanoreactor were supported on the SiN windows, while Al_2O_3 has been used as the support for the Pd particles in the XRD and GISAXS measurements. We have used the *ReactorAFM*, introduced in chapter 2, to obtain in-situ real-space observations on a sample of Pd particles similar to the one used for the XRD and GISAXS measurements, but with a smaller particle diameter of 6 nm and lower coverage of 100 particles/ μm^2. Unfortunately, due to this low Pd coverage it was not possible to measure the turnover rate with mass spectrometry. Calorimetry was also not possible because of the large thermal mass of the sample and sample mounting structure compared to the heat of reaction. Therefore, we cannot be sure whether the reaction was oscillating under the conditions of our AFM observerations.

Figure 7.6 shows an ensemble of Pd particles imaged by non-contact AFM in two different atmospheres and at high temperatures, in both cases close to the phase boundary between metal and surface oxide (figure 7.1). For these images, the rms-roughness of the line profiles on the Al_2O_3 substrate was taken as a measure for the vertical resolution, and this was found to be 0.2 nm. Within this margin, the particle heights did not change when the atmosphere was changed. The horizontal resolution was limited due to convolution of the particle contours with the tip shape, therefore a systematic analysis of the lateral particle shape has not been attempted.

Summarizing the real-space observations of TEM and AFM, it can be concluded that the particles remained largely unchanged. In particular, we can conclude that the particles did not get fully oxidised under reaction conditions. Neither have other effects such as fragmentation, clustering, or particle migration been observed as a direct consequence of the switch from one gas composition regime to the other.

7.3.4 Grazing incidence small angle X-ray scattering

The GISAXS data have been obtained at the ID03 beamline of the ESRF operating at 18 keV using a Maxipix 2D-detector. To optimise the signal-to-noise ratio the GISAXS data have been averaged in the following way. GISAXS patterns have been acquired continuously during several consecutive periods of the reaction oscillation. Each period has been manually segmented into 12 sections, based on the phase of the oscillation using the CO_2 signal as reference and on the intensity in a 20-pixel region

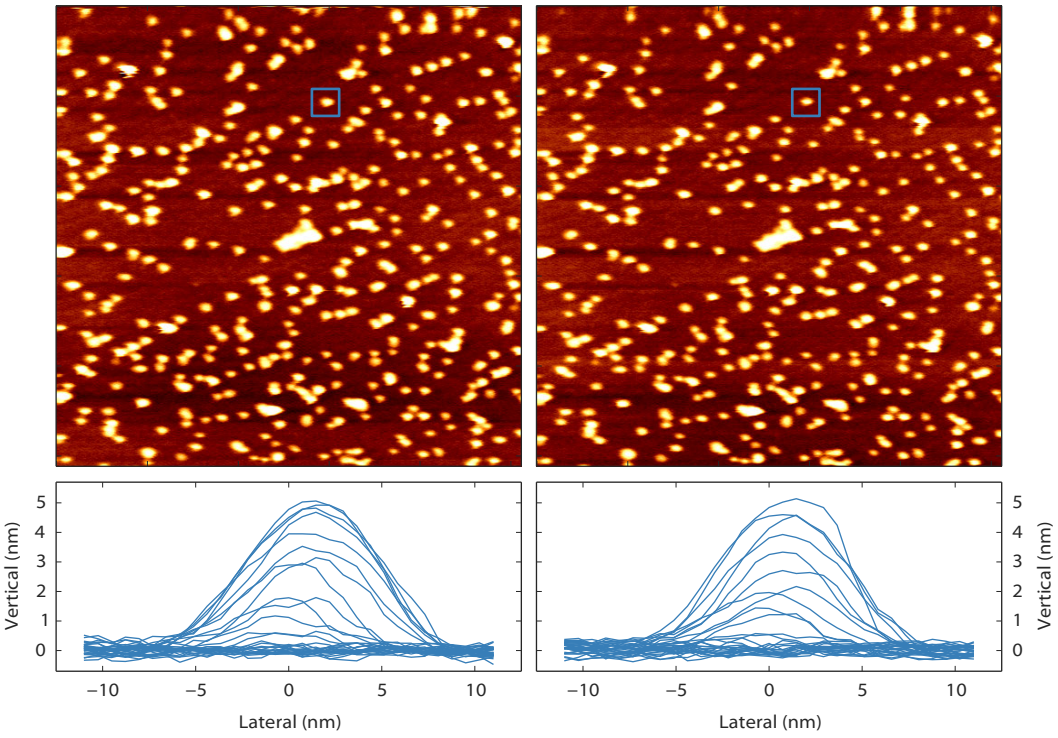

Figure 7.6. The upper panels show 700 × 700 nm^2 non-contact AFM images on size-selected Pd particles supported on α–Al_2O_3, obtained at 475 K and a total pressure of 1 bar. The coverage is about 100 particles/ μm^2, but the particles are distributed inhomogenously over the surface, giving rise to a higher coverage in the region imaged here. The left panels have been obtained in a 1:3 Ar:O_2 mixture, the right panels in a 10:1:30 Ar:CO:O_2 mixture. The AFM was operating in frequency modulation mode with a frequency shift setpoint of +5 Hz and an oscillation amplitude of 5 nm. The lower panels each show 30 horizontal line profiles from the regions indicated by the blue rectangles in the images, proving that the particle height did not change. The cross-sectional particle shape has not been analysed in detail, as it is formed by the convolution of the tip shape with the particle shape.

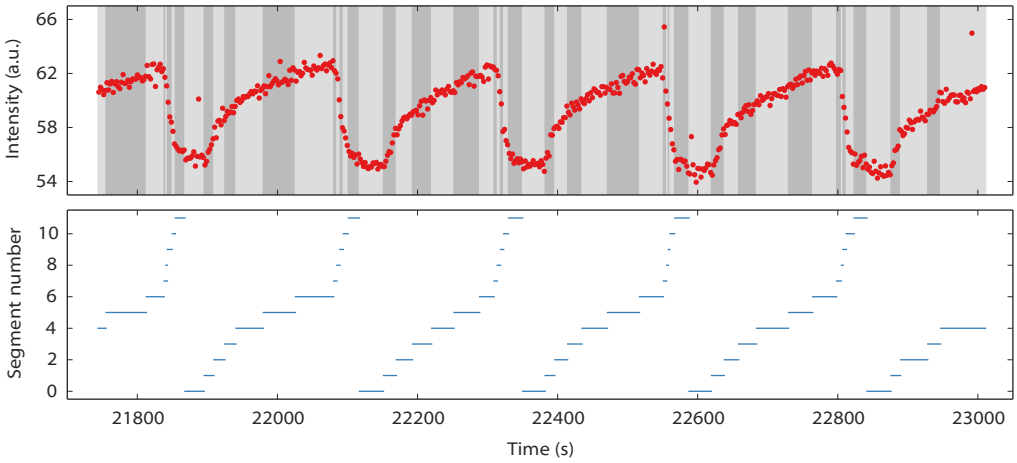

Figure 7.7. The upper panel shows the GISAXS intensity integrated from a small region near the Yoneda peak (see figure 7.8 for details) versus time during five full oscillation cycles. The lower panel and the grey bands in the upper panel show how we have manually classified all GISAXS data into 12 epochs, 6 for the parts of the oscillation cycle during which the GISAXS intensity increased, and 6 for the decreasing parts. In this way, the full data set with multiple oscillations was averaged into a combination of 12 GISAXS patterns, with good signal-to-noise characteristics, together covering the complete oscillation cycle. These 12 patterns were used for the subsequent analysis.

close to the center of the Yoneda peak in the GISAXS pattern. This segmentation is illustrated in figure 7.7. All data within each segment (irrespective of the period it belonged to) was taken together and averaged. Two horizontal lines from the 2D-detector (each line has a width of 0.05 mrad) that cut through the Yoneda peak (as indicated in figure 7.9) were used for a detailed analysis as described below.

The GISAXS pattern showed an intensity that was oscillating along $q_{\parallel}$ in the low-reactivity phase, and a more monotonic profile in the high-reactivity phase (figure 7.9). This change in profile can be interpreted as a change in the abruptness of the electron density profile as a function of radius (figure 7.9). The oscillations are the result of a sharp transition in electron density from metal to vacuum, whereas a broadening of this transition blurs these oscillations. The broadening can be caused by a less compact particle shape (i.e. facets rather than sphere), a wider particle size distribution, or by the formation of a surface layer with a lower electron density. From the GISAXS patterns alone it cannot be concluded which of these three scenarios is at work.

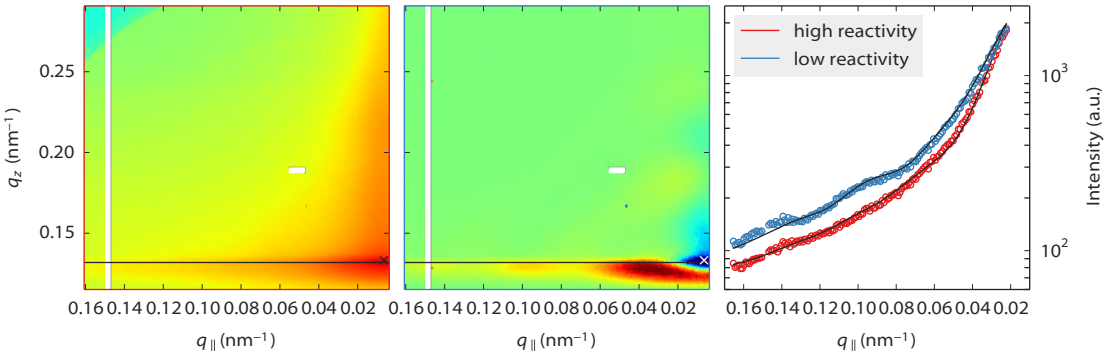

Figure 7.8. GISAXS data after averaging, (left panel) in the high-reactivity regime (logarithmic colour scale), (middle panel) difference signal between the intensity in the low-reactivity regime and that in the left panel, (right panel) linescans through the GISAXS data in the high- and low-reactivity regimes at the location indicated in the left and middle panels. The blue and red curves are the theoretical fits discussed in the text and explained in figure 7.9. The crosses in the lower right of the two GISAXS patterns indicate the location of a 20 pixel ($5 \cdot 10^{-5}$ steradian) region that was integrated to obtain the signal that is shown in figures 7.2 and 7.7.

7.4 Model and interpretation

Having discussed the four sets of experimental data (section 7.3), we now combine all evidence into a consistent model and test this model with numerical fits to the GISASX data in figure 7.8. There were three competing scenarios for the changing electron density profile. A changing particle distribution can be ruled out because the changes were fully reversible (hence the oscillations), and the particle distributions remained also unchanged in the TEM and AFM images. Also faceting is not observed in TEM or AFM. On the other hand, the presence of a PdO oxide was observed in the high-reactivity phase with XRD, in combination with a reduced amount of metallic Pd. The only configuration that is consistent with all these pieces of evidence is one in which an ensemble of relatively compact, metallic Pd nanoparticles is changed into core-shell structures with a Pd core and a thin palladium oxide shell, both under the influence of the deliberate changes in the gas atmosphere (from reducing to oxidizing), and repeatedly during spontaneous reaction oscillations. The electron density of the oxide is lower than that of the metal, hence the blurring of the electron-density profile at the particle-gas interface. When the oxide shell is sufficiently thin, it should be hard to distinguish it in the TEM and AFM images under reaction conditions.

For our numerical fits, we modelled the Pd particles as truncated core-shell spheres on a flat substrate. The core was taken to be metallic (Pd), the shell to be PdO, and the substrate was set to alumina (Al_2O_3). Only three degrees of freedom

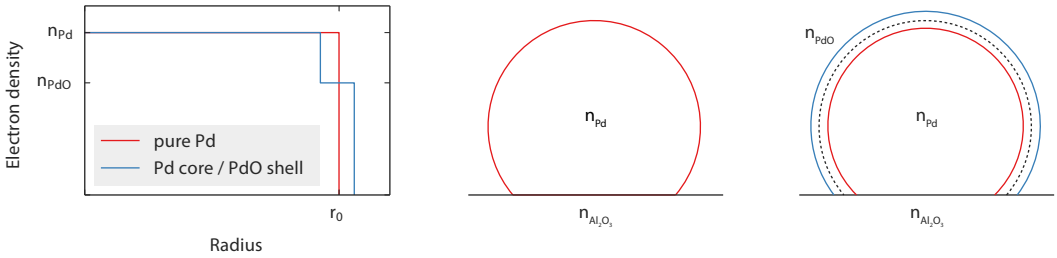

Figure 7.9. The presence of the oscillations along $q_{\|}$ in the line profiles in figure 7.8 correspond to sharp transitions of electron density n from metal to vacuum (as sketched for the pure Pd particle in the left panel). The blurring of these oscillations corresponds to a broader electron density profile. The electron density transition is influenced by particle morphology (e.g. faceted versus spherical shape), particle size distribution, and chemical composition (e.g. $n_{\mathrm{PdO}} < n_{\mathrm{Pd}}$). The model used to fit the GISAXS patterns is that of a spherical core-shell particle on a flat Al_2O_3 substrate having a Pd metal core and a PdO oxide shell (middle, right panels). The fits have been made assuming all variations in the electron density profile can be attributed to changes in the thickness of the oxide shell, while all other parameters (number of Pd atoms per particle, particle size distribution, truncation of sphere) have been forced to adopt constant values throughout the entire oscillation period.

were left in the fit, namely the oxide shell thickness, the total number of Pd atoms per particle, and the parameter quantifying the truncation of the sphere (figure 7.9).

The GISAXS patterns were computed using a formalism for dilute core-shell nanoparticles on a substrate, based on the Distorted Wave Born Approximation[140]. In this approach, particles are treated individually, i.e. there is no scattering process involving multiple particles. To verify that this approximation is appropriate, scanning electron microscopy (SEM) images have been taken of a sample treated similarly to the one analysed here, but with a SiO_2/Si substrate. From these SEM images, the interference function was calculated and this was found to be sufficiently uniform to treat the particles independently in the GISAXS analysis. The Si substrate is not expected to give rise to a significantly different interference function than a Al_2O_3 substrate, and the latter is difficult to image with SEM.

We have developed special Python code in order to fit multiple GISAXS patterns simultaneously, with several shared parameters. This has enabled us to fit the 12 epochs in the average oscillation period in a single step, in which we only allowed the thickness of the oxide shell to vary from epoch to epoch, while forcing the number of Pd atoms per particle and the truncation of the sphere to adopt constant values throughout the entire oscillation period. In this way, internal consistency was ensured and convergence was facilitated, something that could not be done with previously existing software such as IsGISAXS[144].

Since the nanoparticles were not identical but varied slightly in size, each of the three fit parameters was assumed to follow a Gaussian distribution. These

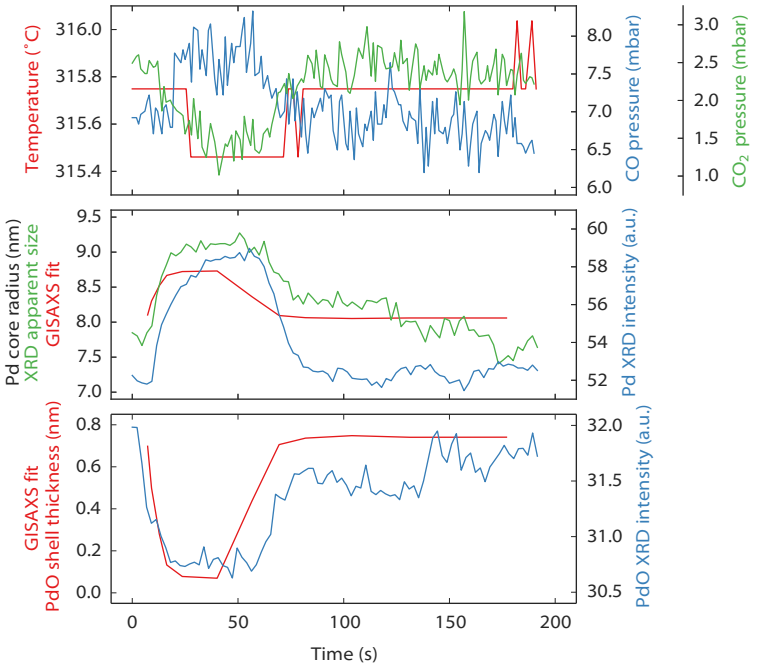

Figure 7.10. Reactivity, GISAXS and XRD data presented over a single oscillation period. Since it was not possible to acquire this complete dataset simultaneously, some curves derive from different periods while the system was oscillating. In particular, the gas composition and sample temperature were measured simultaneously with the Pd metal XRD peak, while the oxide XRD peak and the GISAXS signal were obtained separately. For the GISAXS fit procedure, data from multiple oscillations have been averaged to increase the signal-to-noise ratio (see figure 7.7). To compensate for the slightly different lengths of the periods, the oxide signal has been scaled by 0.978 along the time axis, the GISAXS signal was scaled by 0.789. The apparent particle size from XRD was estimated from the Full Width at Half Maximum (FWHM) of the Pd peak[145], assuming a perfect spherical shape.

distributions were approximated by seven points linearly distributed from $\mu - 2\sigma$ to $\mu + 2\sigma$ and weighted by their relative values of the probability density function. In this way, each simulated GISAXS pattern was constructed as the incoherent sum of 7^3 patterns. A least-squares optimization was then performed on the 28 free parameters (the number of Pd atoms and a sphere truncation parameter, which are kept constant during the 12 phase segments, and a shell thickness for each of the 12 phase segments; all parameters have a mean and standard deviation).

Figure 7.8 shows that the simulated GISAXS patterns obtained with this optimization procedure gave a good fit of the raw data. Figure 7.10 combines the XRD and GISAXS data for an entire period of the spontaneous reaction oscillation. The GISAXS fits are in excellent agreement with the XRD data. Both data sets show that

the high-reactivity phase coincides with the presence of an oxide shell of approximately 1 nm thickness. The corresponding decrease in metal core size, demanded by the fit constraints, matches the decrease in scattering volume corresponding to the reduction in Pd diffraction intensity, while the increase in PdO volume matches the growth in PdO diffraction intensity. Independent confirmation for the reduction of the size of the Pd core during the high-reactivity phase comes from the increase in angular width of the XRD peak from the Pd, which is a direct, inverse measure of the average size over which the metallic component of each nanoparticle extends (figure 7.10, middle panel).

We were unable to get a good fit for the out-of-plane intensity profile of the GISAXS patterns. This could be due to an interface layer between the Pd particle and the Al_2O_3 substrate[138].

7.5 Oscillation mechanism

The periodic formation of the oxide shell seems to indicate a direct analogy to the oscillations observed on the single-crystal surfaces of Pd. However, the observations presented in this chapter provide no information on the feedback mechanism that drives the oscillation on the nanoparticles. Surface roughness played the role of "hidden parameter" on the single crystals, and the roughness-dependent stability of the PdO was the non-linear component required for oscillation. By contrast, TEM and AFM images showed no morphology variations on the nanoparticles. However, roughness on a sub-nm scale, which should be the scale for a nm-thick oxide, would be very difficult to observe, given the resolution of the microscopy images under high-pressure, high-temperature conditions. In addition, roughness can take several forms, ranging from steps on nanoparticle facets (the direct analogue of roughness on single-crystal surfaces), to intermediate surface orientations appearing between the dominant (100) and (111) facets, up to a complete rounding of the particles and a disappearance of the facets. Again, the TEM and AFM images can only be consistent with very modest changes in particle morphology.

Apart from the scenario where roughness is the hidden parameter, we can think of two other candidates for this parameter, although in both cases it is unclear what the non-linear component would be. The first scenario relates to the ongoing discussion about the activity of the PdO, as it is well established that the presence of the palladium oxide correlates with the high-reactivity phase[131, 146], but it is still under debate whether the increased activity should be attributed to the oxide or the oxide should be regarded as a mere consequence of the lower CO partial pressure due to the increased turnover of CO by the metal phase[137, 141, 142, 147–150]. In the latter case, the poisoning of the palladium particles could be the hidden parameter. What speaks somewhat against this scenario is the observation in figure 7.10 that

during the high-reactivity phase neither the thickness of the oxide layer, nor the total amount of PdO seems to increase, which is to be expected for this layer in the self-poisoning scenario. The second possibility for an alternative scenario could be related to the formation of an interfacial PdO layer between the metal particle and the Al_2O_3 substrate[138], which could have a large influence on the activity of the system.

7.6 Conclusion and outlook

Spontaneous reaction oscillations occur during CO oxidation over Pd nanoparticles. These oscillations are accompanied by the periodic formation and reduction of a thin oxide shell on these particles. Further research is required to establish the mechanism of the reaction oscillations. Improved resolution of the in-situ microscopy techniques would be helpful, as this is required to reveal the small morphology variations that probably occur and influence the stability of the oxide. This would establish a key piece of evidence in support of the nanoparticle analogue of the mechanism found for single crystals[131]. Better resolution could be achieved by more stable and sharper tips for the *ReactorAFM*, e.g. made from diamond[151], and by better windows of the TEM nanoreactors, causing less electron scattering, e.g. in the form of 2D-materials such as graphene[152].

Even though this work adds to the debate on the activity of PdO, it cannot pinpoint the cause of the high activity during the presence of the oxide. Recent theoretical work is close to addressing this question for the flat surfaces[142, 149]. The observations presented in this chapter show that this issue is also relevant for nanoparticles, and thus for more realistic catalytic systems.

De Senaatskamer in het Academiegebouw van de Universiteit Leiden[153].